Femtosecond Dynamics of Localized and Continuum States in CdS_xSe_{1-x} Mixed Crystals

J.-C. Merle, A. Daunois, M. Joucla and J.-Y. Bigot

Groupe d'Optique Non-Linéaire et d'Optoélectronique

Institut de Physique et Chimie des Matériaux de Strasbourg

Unité Mixte 380046   CNRS–ULP–EHICS

23, rue du Loess, 67037 Strasbourg Cedex, France

The phase dynamics of the electronic states in the ternary compounds CdS_xSe_{1-x} is investigated under various experimental conditions. At low temperature, the localized states which give rise to an important third-order susceptibility below the band edge, are studied with low intensity laser pulses of a few hundred femtoseconds duration. The excitonic phase dynamics is shown to occur within two different time scales. The first one ($\sim$ 700 fs) corresponds to an exciton-exciton coupling associated with the creation of localized biexcitons. The second decay ($\sim$ 500 ps) is related to radiative recombination and to intraband energy transfer between localized wells. At room temperature, the polarization dynamics of free carriers is studied with 10 fs pulses of high intensity. It is shown that the screening of the Coulomb interaction reduces the scattering rates between electrons. In addition, the electron-phonon interaction appears to be a very efficient mechanism for the intraband energy relaxation of hot carrier distributions initially brought by the ultrashort pulses.

I. Introduction

The coherent light scattering techniques using ultrashort optical pulses are specially well adapted to investigate the primary events that lead to the loss of coherence and population decay in solid state systems like semiconductors or metals. In such systems, the strong couplings between electrons, or between electrons and phonons or crystal defects, broaden the electronic resonances and prevent to determine their intrinsic properties from simple spectral measurements. In the temporal domain, the analysis of the phase decay with femtosecond pulses overcomes this limitation and it has proved very efficient in many studies[1].

In the present work, we are interested in the dynamical properties of the ternary semiconductor compounds CdS_xSe_{1-x}. In these materials, a structural disorder arises from a spatial variation of the sulfur and selenium compositions, which leads to random fluctuations of the crystal potential. At low temperature, this fluctuating potential may trap the excitons, as demonstrated by Permogorov et al.[2] and Cohen et al.[3] who

have shown the existence of localized states with exponential spectral distribution below the free excitons. The dephasing and energy relaxation properties of these localized states differ significantly from the ones of the free excitons. Previous dephasing measurements performed on these mixed crystals have shown that the homogeneous decay time T_2 of localized excitons is of several hundred of picoseconds[4]. More recently, it has been shown[5] that, prior to this long decay, a fast polarization relaxation takes place which is associated with the coherent interaction between localized excitons and biexcitons.

Another interesting aspect of the CdS_xSe_{1-x} compounds is their strong polar character which manifests by important electron-phonon and exciton-phonon couplings. These interactions contribute very efficiently to relax the energy and the phase in these materials. For instance, at low temperature, it manifests by strong luminescence replica, one LO-phonon energy below the main luminescence of the localized states[3,4]. The electron-phonon (and hole-phonon) interaction is also

an important mechanism for the dephasing of free carriers in the band continua as shown recently by studies performed with 10 fs pulses[6]. In this work, the polarization decays have revealed much faster intraband relaxation than in GaAs where the dynamics is dominated by carrier-carrier interactions with important Coulomb screening[7,8].

In this paper, we review the dephasing properties of CdS_xSe_{1-x} mixed crystals under excitation with ultrashort pulses. We first describe the linear optical properties of the localized states (section II). The study of the polarization decay of the excitonic and biexcitonic localized states, at helium temperature with low energy pulses of duration varying from 80 to 500 fs, is reported in section III. The dynamics of the continuum states is then investigated with 10 fs pulses at room temperature under various polarization configurations (section IV).

II. Localized states : Steady state studies

II.1. Introduction

Ternary compounds and especially CdS_xSe_{1-x} have been widely studied for a long time[2,3,9-12]. Their interest is twice : first, the existence of a relatively sharp luminescence band, with a large quantum yield, can be interesting for applications, but unfortunately restricted to the very low temperature domain. Second, composition fluctuations are experienced by the excitons which, by analogy with the electrons in disordered media described by Anderson[13], can be localized. This localization which presents some important differences with the electrons one is, per se, an important domain of fundamental physics.

From the theoretical point of view, the chemical disorder is fully random. The potential fluctuations are like a white noise, having spatial variations at short, intermediate and long ranges. However, in practice, it is not obvious that the chemical disorder follows this model. Two kinds of situations may occur. First, the material can be composed by clusters having very different compositions. This can be easily determined by various techniques. Like the previous groups who have studied these materials, we do not observe any indication of the existence of such clustering. Second, the variation of composition x at medium scale (μm to mm)

can be abnormally large. In such a case, the crystal volume probed in optics is non uniform and the inhomogeneous level broadening is expected to increase, making difficult any precise optical characterization and comparison with the theory.

We have been very attentive to this problem and tried to obtain "homogeneous" crystals. Since this goal has been reached, we will give a detailed description of the sample preparation and present some results of their linear optical properties which allowed us to characterize the localized states in a very accurate manner. We also obtained new informations on the scattering of photons by localized states which can help to complement the existing models.

II.2. Sample preparation

Polycrystalline samples are first synthetized and are subsequently used to grow monocrystalline platelets by a transport method. Great care is taken to obtain pure and homogeneous samples.

For the synthesis, a method proposed by Hemmatt and Weinstein[14] has been adapted. A carbon crucible containing high purity (5N) elements of Cd, S and Se in the desired proportions is introduced in a fused silica tube which is pumped at 10^{-6} torr and sealed. This tube is heated up to 1300 °C at a rate of 60°/hour (except between 500 and 900°C where it is reduced to 20°/hour). Slow heating is used to avoid rapid exothermic reactions and high vapor pressures. The large final temperature is necessary to obtain a product of homogeneous composition.

Samples of CdS_xSe_{1-x} in the entire range of compositions x between 0 and 1 have been obtained. They have been characterized by X-ray diffraction and EXAFS studies[15]. The variations of the lattice lengths a and c with the composition x follow the Vegard's law with a maximum deviation Δx of 5 %. From the width of the observed diffraction lines, it is concluded that the compositional fluctuations are less than 1 %.

A modified Frerichs' method[16] is used to grow the platelets. The polycrystalline material, contained in a small boat of vitreous carbon, is evaporated under an argon flux at 1050 °C in a fused silica tube located in a furnace with a temperature gradient. The platelets grow in the area of the tube where the temperature

is comprised between 600 and 800 °C. They have surfaces of several mm^2 and thicknesses of several μm. A few crystals have thicknesses under 1 μm. To perform characterization or optical studies, well shaped samples presenting nice and uniform surfaces are selected.

The composition of the platelets, determined by X-ray powder diagrams, is comparable, within 1 %, to the one of the original polycrystalline material. Three samples have been studied by energy dispersion X-ray spectroscopy (Delta KEVEX Analyzer) in a JEOL 840 microscope. In this method, a mean volume of 1 μm^3 is analyzed. The fluctuations of composition x on the entire surface are of the order of 1 %, which corresponds to the resolution of the set-up. Some crystals have also been characterized by X-ray diffraction. The scattering volume is of the order of the sample surface multiplied by about 3 μm, which represents an important fraction of the crystal volume. The width of the diffracted lines is comparable to that obtained with good quality GaAs crystals. This indicates that the platelets are free of strain and, taking into account the set-up resolution, that the compositional fluctuations are less than ± 0.5 %.

II.3. Optical characterization

As it is well known, in the wurtzite crystals of CdSSe, the conduction band has a s character and the p-like valence band is decomposed by the spin-orbit interaction and the crystal field[17] in three bands as shown in Fig. 1. Their extrema are located at the Γ point and the optical transitions from these subbands give rise to the A, B and C excitons. The selection rules with respect to the polarization of the incident light $\vec{E}$ and hexagonal axis $\vec{c}$ are the following :

  - transition A is dipole allowed for $\vec{E} \perp \vec{c}$ only

  - transitions B and C are dipole allowed in the two polarizations.

The linear optical properties have been studied on various samples at 2 K. Examples of low temperature transmission and reflection spectra, obtained with a sample of thickness less than 1 μm and of composition $x = 0.36$, are given in Fig. 2. The absorption due to the A and B excitons shows up around 2.02 and 2.05 eV. In reflectance, the main structures are due to interference effects. The minimum of reflectance around 2.02 eV

corresponds to the A exciton [9]. The excitonic structures are broader than in the binary compounds CdS or CdSe because of the reduced lifetime of the free excitons which are easily trapped by the potential fluctuations.
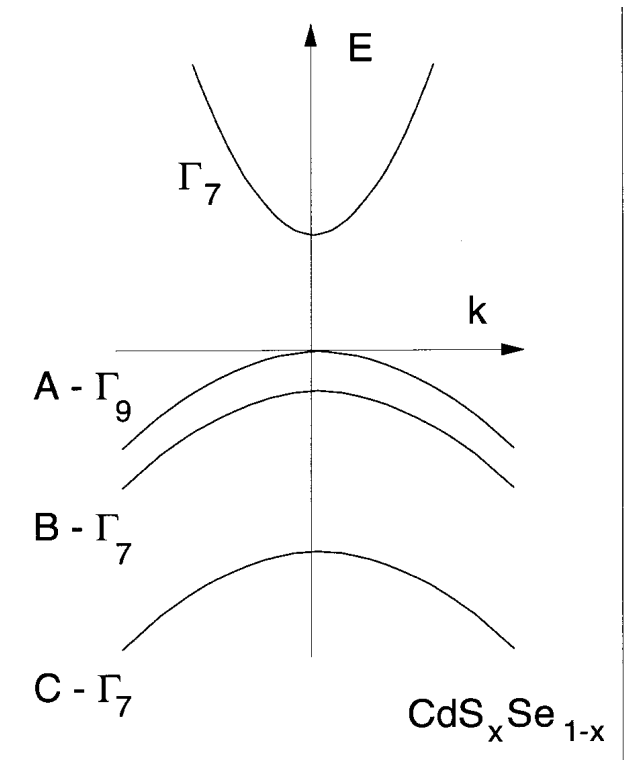

Figure 1. Band structure of CdS$_x$Se$_{1-x}$ with the notations A, B and C used for the transitions starting from the three upper valence bands up to the conduction band.

To characterize the crystallographic quality of the samples, we have studied their birefringence properties. The samples are illuminated by a polarized white light source using a broadband polarizer P. The transmitted light is analyzed with a second polarizer A and is detected with an optical multichannel analyzer after dispersion by a monochromator. The results are corrected for the variation of the detection with A. Three spectra are represented in Fig. 3. For the case 1 ($P \perp \vec{c}$ and $A \perp \vec{c}$, noted $\perp, \perp$), the usual transmission spectrum is obtained. In the case 2 (noted +45°,-45°), P and A are crossed and oriented at ±45° with respect to the $\vec{c}$ − axis. As expected, a large birefringence is observed with a maximum in the transparent region near the A exciton. In case 3 ($P \perp \vec{c}$ and $A \parallel \vec{c}$, noted $\perp, \parallel$), the remnant very weak signal, which is partly due to cryostat imperfections, has an amplitude less than 10^{-3} that of

the signal observed in cases 1 or 2. From these observations, it can be concluded that the direction of the $\vec{c}$ − axis does not fluctuate (on the scale of the entire surface) and that the samples are free of strain.
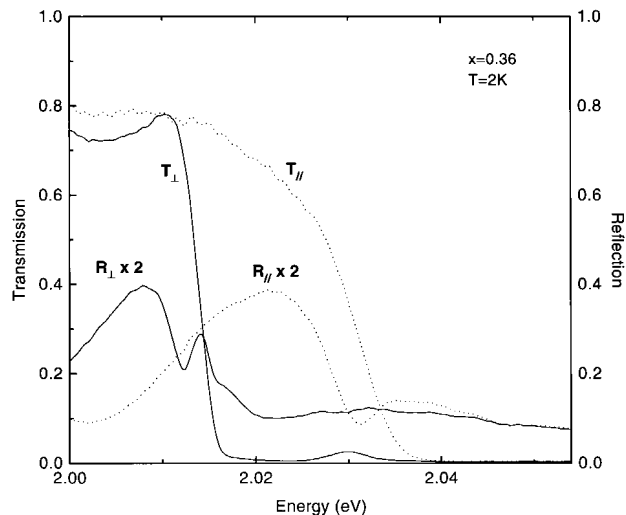

Figure 2.   Transmission and reflectance spectra of $CdS_{0.36}Se_{0.64}$ at 2 K in the two polarizations parallel and perpendicular to the $\vec{c}$ − axis.
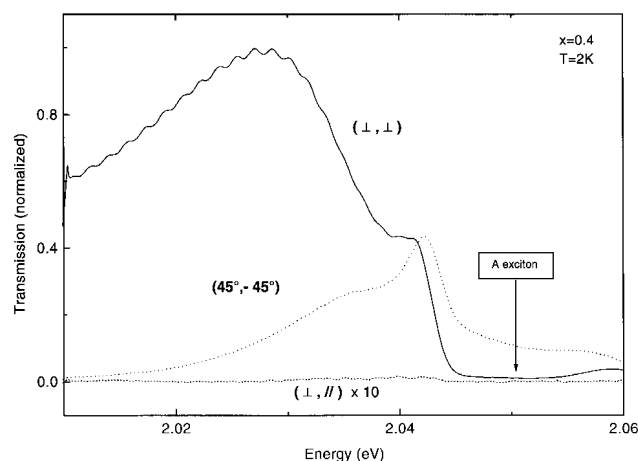

Figure 3. Birefringence spectra of $CdS_{0.4}Se_{0.6}$ at 2 K (see the details in the text).

As previously reported[2,3], we observe, at low temperature, an intense luminescence band located on the low energy side of the A exciton. This is shown in Fig. 4 with two spectrally different cw laser excitations, well above the exciton (curve a) or in resonance (curve b). In both cases, the luminescence is observed in the polarization $\vec{E} \perp \vec{c}$ and the excitation power is of the order of 1 W/cm^2. Phonon replicas are also observed on the low energy side of the figure. Curve a) is characterized

by a width of the main band (6 meV FWHM) which is smaller than generally reported (10 meV or more except in Ref. [11] where the same value is obtained for $x = 0.36$). Consequently, the phonon replicas appear on a very weak tail of the main band (0-phonon band). The sharpness of the luminescence bands, as compared with others, is due to an excellent homogeneity of our samples.
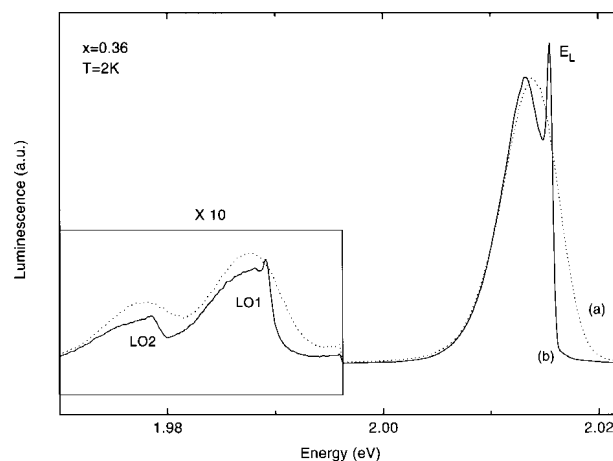

Figure 4. Normalized luminescence spectra of the localized excitons of $CdS_{0.36}Se_{0.64}$ at 2 K. a) nonresonant excitation (above the exciton). b) resonant excitation at the energy E_L.
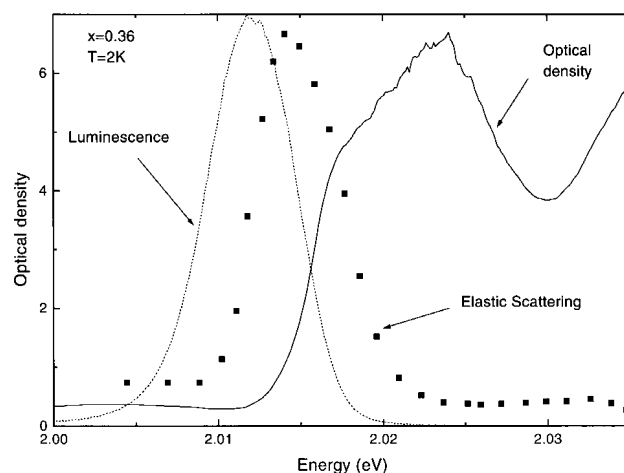

Figure 5. Comparison of the absorption, luminescence and scattering spectra of $CdS_{0.36}Se_{0.64}$ at 2 K.

Curve b) of Fig. 4 corresponds to a resonant excitation with a monochromatic source which position corresponds to the sharp peak noted E_L. Several studies devoted to the resonant luminescence excitation lead to the following description[2,3,12]: on the low energy side of the free excitons (extended excitations) there exist

localized states associated with the potential fluctuations. By decreasing the energy, these states are more and more localized. Due to the random character of the fluctuations, their density decreases continuously. The most energetic states (free or weakly bound states) are easily trapped on deeper levels, the main mechanism of energy relaxation being an inter-well tunneling by acoustic phonons. For deep states, the above processes are considerably attenuated because of the large distances between the traps. This model explains the important energy shift between the luminescence and the maximum of absorption corresponding to the free excitons (see Fig. 5). In the case of resonant excitation, bound excitons are directly created at the laser energy E_L. If N_L represents the number of incident photons per second in the energy interval ΔE_L, the number of absorbed photons is equal to $\alpha * N_L * \mathcal{D}(E_L) * \Delta E_L * P_r(E_L)$, where P_r is the (mean) absorption probability per second, $\mathcal{D}$ the density of states and α a coefficient with a temporal dimensionality. The excited states loose energy by radiative and non-radiative processes with respective probabilities per second P_r and P_{nr}. In a steady state experiment, a mean occupation number per state n_{oc} is obtained from the balance equation :

$$\alpha * N_L * \mathcal{D}(E_L) * \Delta E_L * P_r(E_L) = n_{oc}(E_L) * \mathcal{D}(E_L) * \Delta E_L * [P_r(E_L) + P_{nr}(E_L)]$$

which leads to :

$$n_{oc}(E_L) = \frac{\alpha * N_L * P_r(E_L)}{P_r(E_L) + P_{nr}(E_L)}$$

The above equalities are verified as long as a linear regime is valid without saturation effects. We have verified that it is the case in the domain of excitation that we have studied (i.e. some W/cm^2).

The number of emitted photons in the interval ΔE_L is given by :

$$N_S = \frac{\alpha * N_L * \mathcal{D}(E_L) * P_r(E_L)}{1 + [P_{nr}(E_L)/P_r(E_L)]} \qquad (1)$$

This mechanism gives rise to the sharp line of Fig. 4, curve b). It is presently described as a "resonant fluorescence" due to localized states spacially distributed at random. It can be also understood as a Rayleigh scattering, as the material is inhomogeneous at the scale of potential fluctuations. For energies corresponding to extended states, the scattering is expected to be mostly directed in the forward direction and it disappears in the free exciton region.

The non-radiative processes introduced in Eq. (1) are mostly due to the above mentioned scattering by acoustic phonons. At $T \simeq 0$ K, they contribute to fill deeper states ($E < E_L$) and the number of emitted photons per unit time and per unit energy is given by :

$$N_{\text{LUM}}(E) = \mathcal{D}(E) * n_{oc}(E) * P_r(E) \qquad (2)$$

As seen in Fig. 4, the shape of the luminescence bands obtained by resonant and non-resonant excitations is similar for $E < E_L$. This is true for any E_L located in the luminescence band, except, however, for the lowest energies[2,3,18]. This indicates that the energy relaxation involves very small quanta (< 1 meV). As $P_r(E)$ is expected to be independent of E, except for tightly bound states, the luminescence shape gives information on the product $\mathcal{D}(E) * n_{oc}(E)$. A comparison between the luminescence and the scattering gives more informations on $\mathcal{D}$ and n_{oc}, as discussed later.

Coming back to Fig. 4 curve b), it must be noted that the Rayleigh line cannot be entirely attributed to the compositional fluctuations. Surface and bulk defects (impurities, dislocations...) also play a role. It is this spurious contribution which renders difficult the observation of Raman and Brillouin scatterings. In previous studies[2,3], intense Rayleigh scattering has prevented a detailed shape analysis of the main luminescence band, an analysis which has been restricted to the phonon replicas. Thanks to the good quality of the samples, we observe weak Rayleigh lines. The variation of the scattered intensity with energy is reported in Fig. 5. A sharp resonance attributed to the localized states is observed, superimposed on a weak background

which intensity depends on the laser spot position on the sample and which we attribute to surface defects.

It is instructive to compare the three curves plotted in Fig. 5. With very thin samples (less than 1 μm), the absorption can be measured even in the free exciton region. On the low energy side, the absorption is proportional to the density of states (as we did not make reflection corrections, this is only true for OD >2). It can be noted that a variation of the density of states of the form $\mathcal{D}(E) \propto \exp\left[-\frac{E-E_x}{\delta}\right]^{\beta}$, where E_x is the free exciton energy and δ an activation energy, is certainly not true in the entire range between E_x and E_x - 20 meV for a single constant β which characterizes the localization process. It is very likely that a better description has to take into account higher order site to site correlations. Let us now compare the luminescence and scattering curves. At low energies, where the non-radiative processes are inefficient, the scattering, according to Eq. (1), is proportional to $\mathcal{D}(E)$. In this region, the luminescence dominates since the occupation number n_{oc} of Eq. (2) is large. For higher energies, n_{oc} decreases and the scattering is favoured with respect to the luminescence. For still higher energies, the large non-radiative probabilities P_{nr} are responsible for the decrease of the scattering.

All these observations are in good agreement with the accepted description of energy tranfer and dynamics in the bound state region. In addition, the scattering measurements reported here bring new information which will be analyzed more quantitatively in a forthcoming paper.

III. Polarization decay of localized states

The localized density of states can be viewed as an inhomogeneously broadened distribution of excitons trapped in potential wells of different depths. Their coherent dynamics is therefore expected to be very long, at least for the less energetic ones in the deep wells, since the probability of being perturbed by phonons or impurities is reduced during their lifetime. Long dephasing times have indeed been measured in such systems [4, 19]. These studies have reported dephasing times ranging from 400 ps on the high energy side of

the localized density of states down to 2.2 ns on the low energy side[19]. These decay times are close to the localized exciton lifetimes as measured with time resolved photoluminescence spectroscopy[20, 21]. However, such decay behavior does not take into account the two-particle effects that may occur when biexcitons are created by two-photon transitions. It is the aim of this section to show how such effects lead to a fast initial decay of the polarization. We first describe the measurement technique and the results and then discuss the two-particle effects.

III.1. Photon echo studies of the localized states

The photon echo (PE) measurements are performed in the self-diffracted and stimulated configurations with femtosecond optical pulses. In the first case, the signal is measured in the direction $2\mathbf{k}_1 - \mathbf{k}_2$ as a function of the relative delay ΔT_{12} between the two incident pulses of wave vectors $\mathbf{k}_1$ and $\mathbf{k}_2$. In the stimulated or three-pulse configuration, the signal $\mathbf{k}_1 + \mathbf{k}_3 - \mathbf{k}_2$ is detected either as a function of ΔT_{12} (coherent dynamics) or ΔT_{13} (population dynamics)[22]. The low energy pulses (50 pJ) are produced by a modified CPM cavity that allows ajustable pulse duration (80-500 fs) and a slight tunability (central wavelengths between 605 and 625 nm). The temporal delays are made with micrometric stepper motors (0.1 μm per step) and the detection is performed with a photomultiplier and a standard synchronous lock-in technique with double chopping of the incident beams. The samples are immersed in pumped liquid helium at 2 K. Great care is taken of the polarization properties of the incident pulse with respect to the sample $\vec{c}-$ axis. As shown below, the low peak power is crucial in these experiments in order to avoid the strong exciton-exciton collision regime. Another important aspect is the low Rayleigh scattering of the samples described in the preceding sections (Fig. 4). This allowed us to explore exciton densities ranging between 10^{13} and 5×10^{14} cm^{-3} as estimated by taking into account the sample absorption and assuming a quantum efficiency of 1.

Fig. 6a shows the PE measurements obtained in the two-beam configuration with a 0.6 μm-thick

$CdS_{0.35}Se_{0.65}$ sample, the laser frequency being in resonance with the localized excitons. This signal displays a fast oscillatory decay and a much longer one which persists during several hundreds of picoseconds. The slow component corresponds to the loss of coherence of the excitons trapped in the spatially fluctuating crystal potential. It is similar to the one reported in the dephasing measurements performed with picosecond pulses[4,19]. Two mechanisms are involved in this decay. In the deeper wells, the phase and energy relaxation of the excitons can occur only via radiative band to band recombination. In this case, the dephasing time T_2 is close to $T_1/2$ as for atomic two-level systems : the phase coherence is destroyed by interband spontaneous emission. For the localized states with higher energy, intersite exciton-phonon scattering may occur leading to intraband energy relaxation. In this mechanism, the hopping of excitons from one site to another is assisted by acoustic phonons. It involves tunneling of the excitonic wave between the non-communicating localization sites.

In Fig. 6b, the slow picosecond decay has been deconvoluted. The fast exponential decay is seen to occur within about 600 fs. This time has been measured on many samples using different incident laser intensities. It is comprised between 600 and 700 fs and has almost no intensity dependence. This is shown in Fig. 6c where the decay varies between 650 and 700 fs for a variation of the laser intensity over one decade. The intensity I_{max} corresponds to an estimated exciton density of 2×10^{14} cm^{-3}. The difference between Figs. 6b and 6c is mostly due to the different pulse durations which are respectively 80 and 400 fs. The corresponding different spectral contents of these pulses explain the different magnitudes in the initial coherent peak around zero delay. It is higher in Fig. 6b since the power spectrum of about 10 nm extends above the localized density of states where the dephasing dynamics is shorter (see the discussion of Fig. 10).

The oscillations appearing in the photon echo decay have a period of 800 fs. Different sample compositions x between 0.32 and 0.4 have revealed the periodicity. It is worth noticing that, for the highest

pulse intensity in Fig. 6c, the contrast of these oscillations increases, indicating that they are favoured by multiparticle excitation. In addition, measurements performed at temperatures above ~ 15 K show no oscillations confirming that the underlying process is related to localized states. As demonstrated in the following paragraph, they correspond to quantum beats associated with the creation of localized biexcitons. Before discussing this beating behavior, we would like to emphasize that the fast 600 fs and slow components are both characteristic of the localized density of states with low densities of excitation. Measurements performed with much higher peak powers corresponding to exciton density up to 10^{17} cm^{-3} show much faster decay times. This was checked using 80 fs pulses amplified by a copper vapor laser. The corresponding self-diffracted photon echo obtained at $T = 2$ K is displayed in Fig. 7a. In this case, the polarization decay is faster than the temporal resolution. This is due to strong exciton-exciton interactions which act as an efficient dephasing mechanism. Similar observations have been reported in bulk GaAs[23] or in GaAs/GaAlAs quantum wells at room temperature[24]. Above helium temperature, in addition to the vanishing beating behavior, faster decays are obtained even at low excitation densities. In this case, it is the thermal activation of the localized excitons outside the potential wells which destroy their phase coherence. This regime of exciton-phonon scattering becomes more and more efficient as the temperature is increased leading to decay times of ~ 70 fs at 295 K, as shown in Fig. 7b with a pulse duration of 60 fs. Here, we have used the stimulated three-beam configuration in a $CdS_{0.5}Se_{0.5}$ sample. This composition was necessary due to the band gap shift with temperature. The asymmetric decay obtained for positive and negative temporal delays indicate that the signal corresponds to a polarization free decay rather than to a photon echo. This behavior which is characteristic of a homogeneous linewidth[25] shows that the inhomogeneous localized states have little influence at high temperatures, in agreement with the linear properties reported in Section II.
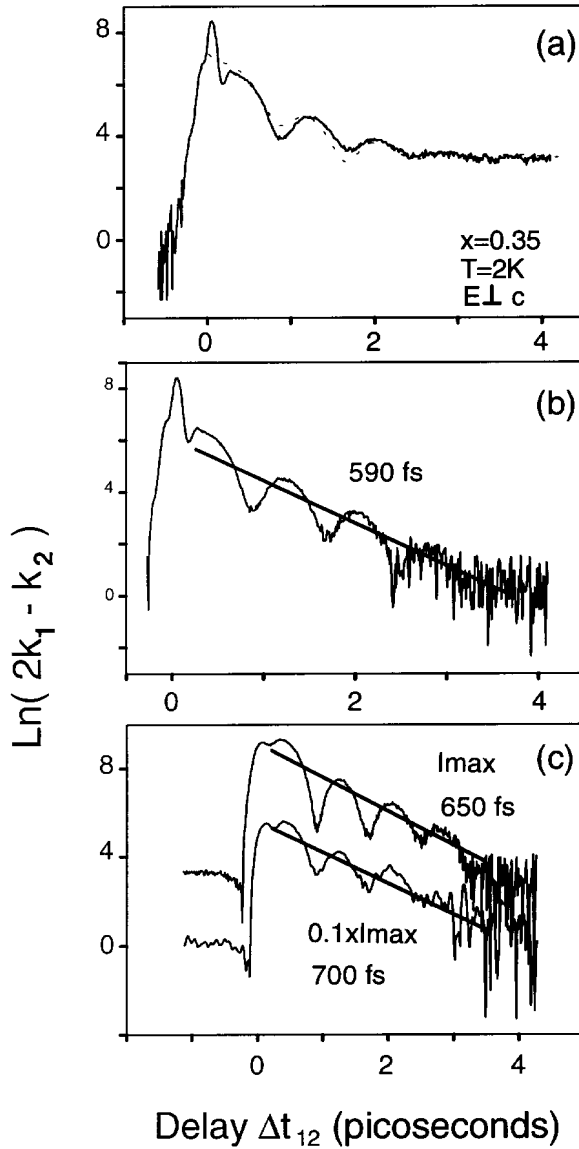
Figure 6. Integrated photon echo signal. a) Full signal (solid) and theoretical fit (dotted) with parameters given in the text. b) Deconvoluted fast decay component. c) Fast decay behavior as a function of incident intensity for an excitation by 400 fs pulses. I_{max} corresponds to a localized exciton density of 2×10^{14} cm^{-3} which is also valid for a) and b) curves.

III.2. Localized biexcitons and quantum beats

The 800 fs periodic oscillations in Fig. 6 are due to quantum beats involving a two-particle state. This is proved by luminescence measurements under band to band pulsed excitation. Fig. 8 shows a series of normalized luminescence spectra obtained for various laser intensities. At low excitation densities ($N < 10^{13}$ cm^{-3}), the luminescence spectrum of the localized excitons is quite similar to the one obtained under band to band

cw excitation (Fig. 5). At higher intensities, a shoulder develops on the low energy side which is super-linear with increasing laser intensity. The optical transition corresponding to this new luminescence "structure" involves two photons. This is shown in Fig. 9a where we have plotted the luminescence intensities measured at the spectral positions corresponding to the peak and to the structure as a function of the incident power. The slopes 1 and 2 are characteristic of one- and two-photon processes.
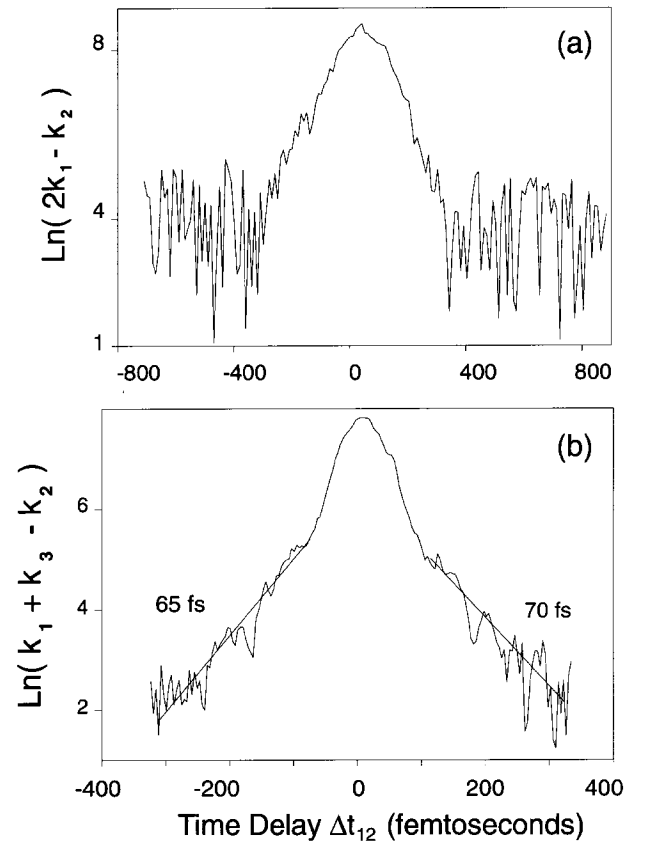

Figure 7. Photon echo signals obtained in different experimental conditions. a) CdS$_{0.35}$Se$_{0.65}$ at 2 K with 80 fs amplified pulses giving an exciton density of about 10^{17} cm^{-3}. b) CdS$_{0.5}$Se$_{0.5}$ at room temperature and at low excitation density in the stimulated three-beam configuration.

The 5 meV energy separation ΔE between the two luminescence structures in Fig. 8 is close to the binding energy of the biexcitonic state in the binary compounds CdS (5.4 meV) and CdSe (4 meV)[26]. The two-photon process observed in Fig. 9a is therefore very likely related to the creation of localized biexcitons. The corresponding energy diagram is displayed in Fig. 9b where the optical transitions for the one- and two-photon pro-

cesses are represented. The oscillations are due to quantum beats between the two probability transitions : $|g\rangle \longrightarrow |ex\rangle$ and $|ex\rangle \longrightarrow |biex\rangle$. The beat period ΔT is proportional to the inverse biexciton binding energy $\Delta E = E_{\mathrm{Bi}} - 2E_{\mathrm{x}}$: $\Delta T = h/\Delta E$.
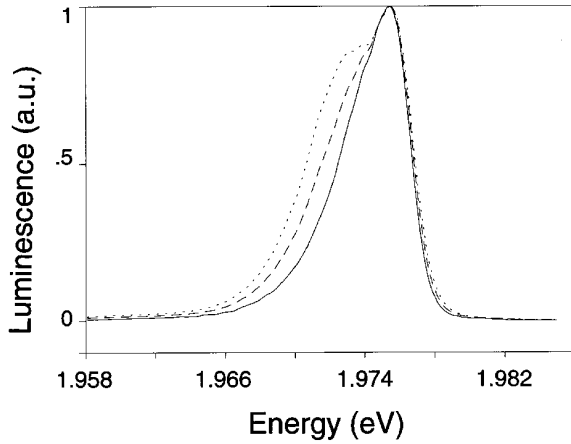

Figure 8. Localized states luminescence as a function of CPM laser intensity for 2, 20 and 100 pJ pulse energies (full, dashed and dotted curves, respectively).

Quantum beat spectroscopy has proven to be a useful technique to probe the coherent dynamics in the femtosecond time scale. As in atomic spectroscopy[27], quantum beats result from interferences between the amplitude transitions of coherent states. It has been recently extended to ultrashort pulse techniques in various systems to probe the coherent motion of molecules[28] or of lattice vibrations[29] or energy splittings in semiconductors[30,31]. It has also revealed the existence of biexcitons in GaAs quantum

wells[32]. We have modeled the coherent dynamics of the exciton-biexciton problem using the optical Bloch equations applied to a three-level system. Assuming $\delta -$ function pulses, we obtain for the time dependent third order polarization in the case of the self-diffracted configuration :
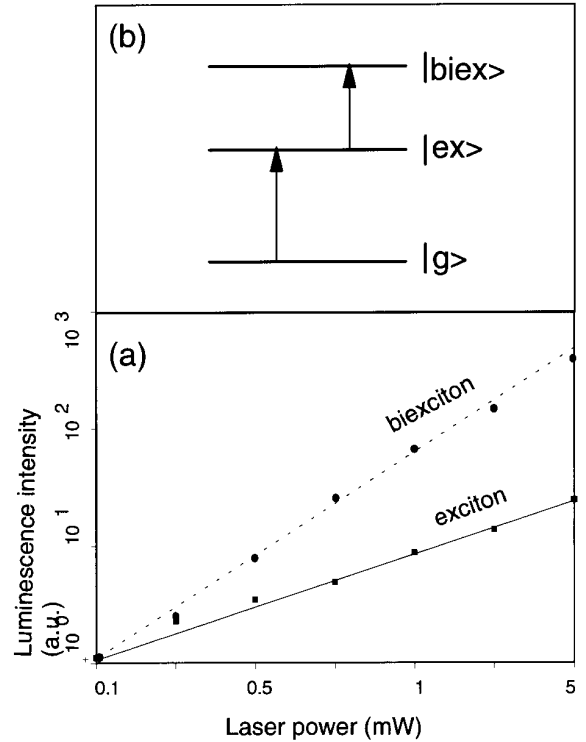

Figure 9. a) Luminescence intensity as a function of incident intensity showing the one- (full curve) and two- (dotted curve) photon processes. b) energy diagram of the corresponding optical transitions.

$$P^3(t,\tau) = \frac{i}{4\hbar^3} |\mu_{\mathrm{ex}}|^4 \exp(\Omega_{\mathrm{ex}}^* \tau) \left[\exp(\Omega_{\mathrm{ex}} t) - \frac{\alpha}{2} \exp(\Omega_{\mathrm{bi}} t) \right] \tag{3}$$

with $\Omega_{\mathrm{ex}} = -\dfrac{i}{\hbar}(E_{\mathrm{ex}} - \hbar\omega) - \dfrac{1}{T_2^{\mathrm{ex}}}$, $\Omega_{\mathrm{bi}} = -\dfrac{i}{\hbar}(E_{\mathrm{bi}} - E_{\mathrm{ex}} - \hbar\omega) - \dfrac{1}{T_2^{\mathrm{ex}-\mathrm{bi}}}$ and $\alpha = \left| \dfrac{\mu_{\mathrm{bi}}}{\mu_{\mathrm{ex}}} \right|^2$. The star denotes complex conjugation. $\hbar\omega$ is the central frequency of the incident pulses, T_2^{ex}, $T_2^{\mathrm{ex}-\mathrm{bi}}$ are the dephasing times and μ_{ex}, μ_{bi} are dipole moments of the corresponding transitions. τ represents the time

delay ΔT_{12} between pulses 1 and 2. Only the resonant transitions $|g\rangle \longrightarrow |ex\rangle$ and $|ex\rangle \longrightarrow |biex\rangle$ have been considered in Eq. (3). The two-photon process $|g\rangle \longrightarrow |biex\rangle$ is neglected since it brings a contribution only on the negative delays[33]. It brings an additional resonance which, in the spectral domain, is given by $\Sigma(2\omega) = |E_0(\omega)\mu_{\mathrm{bi}}|^2 / (E_{\mathrm{bi}} - 2\hbar\omega + i\hbar\Gamma_{\mathrm{bi}})$, and

modifies the one-photon polarizations P_{ex} and P_{ex-bi}

according to [34]:

$$P_{ex}(\omega) \sim \frac{|\mu_{ex}|^2 E_0(\omega)}{i\hbar\Omega^*_{ex} - \Sigma(2\omega)} \quad ; \quad P_{ex-bi}(\omega) \sim \frac{|\mu_{bi}|^2 E_0(\omega)}{i\hbar\Omega^*_{bi} - \Sigma(2\omega)} \qquad (4)$$

For an inhomogeneous medium, the photon echo is obtained by integration of the polarization over the dipole distribution and integration in real time t leading, in the case of infinite inhomogeity, to the signal:

$$S(\tau) \sim (1 + \beta^2 - \beta\cos\Omega\tau) \exp\left(-\frac{4\tau}{T_2^{ex}}\right) \quad (5)$$

with

$$\beta = \alpha\exp\left[-\tau\left(\frac{1}{T_2^{ex-bi}} - \frac{1}{T_2^{ex}}\right)\right]$$

and $\hbar\Omega = E_{bi} - E_{ex}$. Using Eq. (5) with the experimental values $T_2^{ex-bi} = 700$ fs, $T_2^{ex} = 500$ ps, $\Omega = (2\pi/830)$ radfs^{-1} allows to fit the echo decay (dotted curve in Fig. 6a). The only adjustable parameter is α which represents the two-photon enhancement factor. We used $\alpha = 6$ which is a reasonable value as compared, for instance, to CuCl ($\alpha = 20$) [35]. The lower value found here indicates that the extension of the biexcitonic wave function is reduced as compared to CuCl, which is consistent with the fact that we are considering localized biexcitons.

Additional important remarks have to be made. The first one concerns the inhomogeneous nature of the exciton-biexciton system. The derivation of Eq. (5) is obtained under infinite inhomogeneity. In fact, one should consider a finite density of localized states which, for instance, can be modelled by $\mathcal{D}(\hbar\omega) = \mathcal{D}(E_x)\exp\left[-\frac{E_{ex}-\hbar\omega}{\delta}\right]^{\beta}$ where β is a parameter that depends on the localization process and δ an energy that characterizes the fluctuating potential felt by the exciton. E_{ex} is the "free" exciton energy associated with the virtual crystal. Taking into account this finite distribution does not affect the dynamics as long as the inhomogeneous broadening is larger than the pulse spectrum. To evaluate the influence of such spectral distributions, we have made photon echo measurements

by tuning the pulse in the region of the localized states. This was made in the stimulated configuration in order to distinguish between homogeneous and inhomogeneous effects (the signal being temporally symmetric in the first case and asymmetric in the second case[25]). The results are shown in Fig. 10. The top curves represent the pulse spectra for three different situations together with the localized states luminescence (dashed curve). The corresponding signals $k_1 + k_3 - k_2$ are represented below for the early times. The signal (a) corresponds to a pulse tuned in resonance with the free exciton, above the localized density of states. As expected, in this case, the signal is symmetric in time since the exciton is homogeneous at this low temperature and decays very rapidly within 280 fs. The case (b) corresponds to the resonant excitation of the localized states. Quantum beats are observed as in Fig. 6 where the entire dynamics is better displayed. In the case (c), the tail of the bound states is excited. The weak observed signal is asymmetric and therefore corresponds to an inhomogeneous distribution. One can notice the absence of oscillations which seems contradictory with the fact that localized states of lower energy are excited, where one would expect to be in a more favourable case to reinforce the exciton-exciton coupling. In fact, the properties of these states (dipole moment, coupling with the phonons...) may appreciably deviate from those of less bound states observed in case (b). Even for the lowest states which contribute to the luminescence, there are experimental evidences[2,12] for such deviations. A fortiori, this can be expected for even lower energy states. The absence of oscillations can be tentatively explained by supposing that the relative population of excitons and biexciton populations do not favour beatings. Because of the weakness

of the signal, a study of the dependence of the signal with the laser intensity was not possible. It can also be supposed that a dependence of the biexciton binding energy versus the localization energy is responsible for this absence of oscillations.
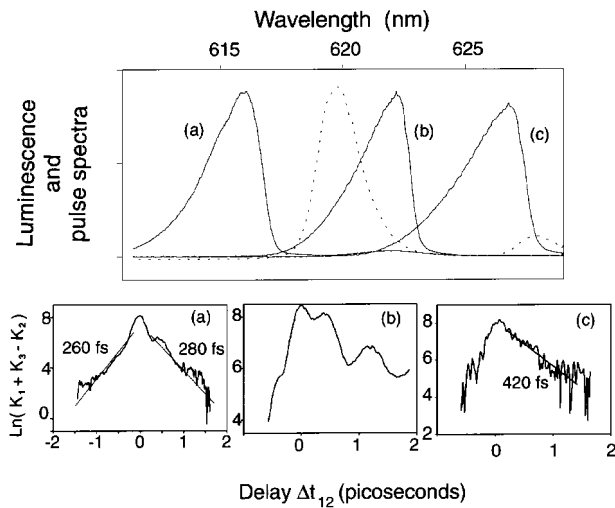

Figure 10. Selective spectral excitation of a $CdS_{0.35}Se_{0.65}$ sample at 2 K. Top) Luminescence (dotted curve) and pulse spectra for a) high (resonant with free excitons states), b) medium (resonant with the localized states) and c) low energy laser excitations. Bottom) Corresponding three-beam photon echo signals as a function of the delay ΔT_{12} between pulses 1 and 2.

IV. Continuum states dynamics

This part is devoted to a "problematic" which is very different from the ones of the preceding sections. We are now concerned with experiments performed at room temperature where the localized states are inefficient because of their weak activation energies compared to kT. The laser pulses have much more energy and create high densities of carriers. The excitation is deliberately above the band gap in order to create carriers (electrons and holes) in a non-equilibrium state. Their dynamics is governed by screened carrier-carrier interactions and by phonons which are responsible for their thermalization. Because of their large population and of their non-equilibrium state, the carriers have very fast phase and population dynamics. For this type of experiments, ultrashort pulses of 10 fs duration are required. Consequently, only few experiments have been reported[7,6].

For the theoretical part, the number of works is also very restricted. The difficulties are numerous since one must take into account many body interactions (screened Coulomb interaction of fermions) and electron-phonon interaction. The response of such systems to ultrashort pulses is also a complicated problem. Much work is being carried out in this field using different theories among which the quantum kinetics approach of the Frankfurt group represents an important contribution[36−39].

IV.1. Continuum states dynamics : Phase relaxation

For these experiments, the wave mixing configurations are similar to the ones described in the preceding section. But, the pulses from the CPM oscillator are now amplified by a copper vapor laser operating at 5 kHz. The amplified pulses are then compressed to 10 fs with a system of fiber, gratings and prisms[40].

The pulse spectrum is displayed in Fig. 11 with the absorption spectra of a 0.4 μm-thick single crystal at room temperature in the two polarizations $\vec{E}\perp\vec{c}$ and $\vec{E} \parallel \vec{c}$. The curves are not corrected for reflectivity and this explains the low energy part where Fabry-Pérot fringes can be seen. With the scale used in Fig. 11, the A and B transitions cannot be resolved. The C gap is more contrasted for $\vec{E} \parallel \vec{c}$ than for $\vec{E}\perp\vec{c}$.

The variation of the two-beam four wave mixing (FWM) signals versus the time delay ΔT_{12} is represented in Fig. 12 for different pulse intensities. The experiment is performed in the geometry $\vec{E} \parallel \vec{c}$ with a sample of composition $x = 0.35$ so that the B transitions are principally excited. The estimated carrier densities N vary between 8×10^{16} and 10^{18} cm^{-3}. In addition to the coherent signal centered at zero delay, exponential decays can be observed except for the highest intensity. This decay has an increasing slope with the laser intensity. For the highest intensity, the temporal resolution of the set-up is reached but the signal is still asymmetric and different from the expected coherent spike which should reproduce the pulse autocorrelation profile. A clear decrease of the response time versus the carrier density is observed. It is attributed to electron-electron collisions. For the highest densities N, a non-exponential behavior is observed but a quantitative description of the signal is unfortunately not yet

possible since the decay times fall below the resolution of the set-up. This non-exponential behavior could be the onset of non-Markovian processes as theoretically predicted by Gurevich et al.[41] and El Sayed et al.[39]. We are trying to explore this ultrafast collision regime.
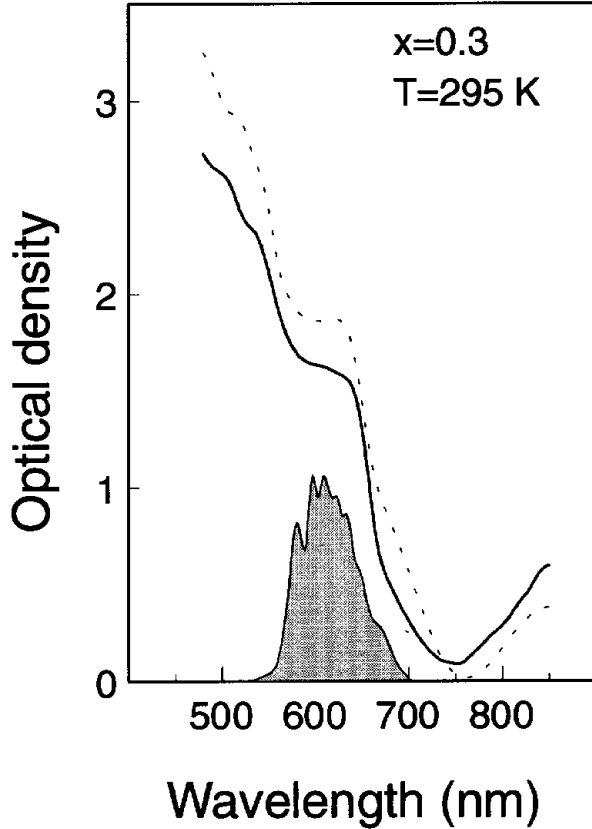

Figure 11. Room temperature absorption spectra in the two geometries $\vec{E} \parallel \vec{c}$ (dotted line) and $\vec{E} \perp \vec{c}$ (full line) for a 0.4μm-thick $CdS_{0.3}Se_{0.7}$ sample. The hatched area represents the spectrum of the 10 fs pulse.

To analyze these results, we assume that a continuum produces a spectral inhomogeneous distribution and that the incident pulses are δ-shaped. The FWM signal should decrease proportionally to $\exp(-4\Delta T_{12}/T_2)$ [25]. The calculated dephasing times T_2, indicated in Fig. 12, correspond to decay times varying between 68 and 16 fs, and their variation versus the carrier density N is plotted in Fig. 13. The observed variation law has a form $T_2 \propto N^{-0.72}$ which differs consequently from the law $T_2 \propto N^{-1}$, expected for unscreened electron-electron interaction. Therefore, this difference shows the importance of screening in this material. Nevertheless, it is less important in CdSSe than in bulk GaAs where similar experiments have given a

$T_2 \propto N^{-0.3}$ law[7]. This difference can be tentatively attributed to the stronger electron-hole correlation in II-VI compounds which present stronger excitonic effects. Such a reduction of the long range Coulomb interaction has also been observed in quasi-2D II-VI systems, $CdZnTe/ZnTe$ [42] as compared to III-V quantum wells, $GaAs/GaAlAs$.
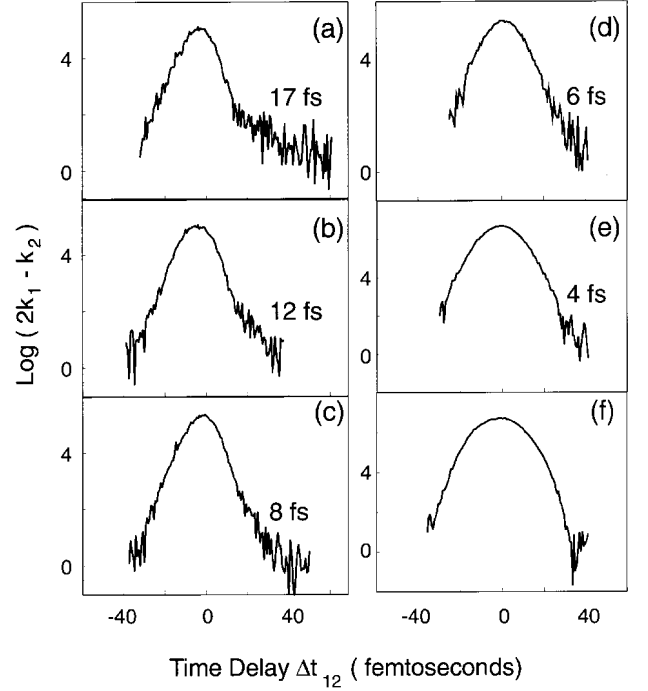

Figure 12. Two-pulse four-wave mixing signals of $CdS_{0.35}Se_{0.65}$ for different carrier densities N at room temperature. (a) to (f) : $N = 0.08, 0.13, 0.2, 0.35, 0.55, 1 \times 10^{18}cm^{-3}$.

To conclude this paragraph, it is worth noticing that in spite of the experimental difficulties and of the crude approximations done in analyzing the data, general tendencies are emerging. It remains to hope that it will stimulate more theoretical investigations in this field.

IV.2. Continuum states dynamics : Population decay

The preceding phase measurements involve the continuum states with high kinetic energies in the conduction and valence bands. In addition to the Coulomb interactions between electrons and holes, electron-phonon (and hole-phonon) scatterings also contribute to the loss of phase coherence. This process leads to the thermalization of the initially non-thermal carrier distribution and can therefore be observed via the population

relaxation. It is expected to be efficient in CdSSe mixed crystals due to the high polar character of this semiconductor family.
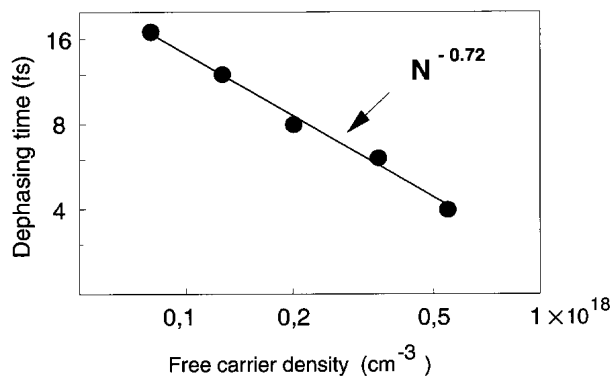

Figure 13. Variation of the dephasing time T_2 with the free carrier density.

In order to investigate the importance of the carrier-phonon scattering mechanism, we have performed stimulated photon echoes using three 10 fs pulses. In this configuration, we varied the optical delay between pulses 1 and 3 to follow the intraband population dynamics. In addition, we made pump-probe measurements using uncompressed 60 fs pump pulses and 10 fs probe pulses. In this case, a selective spectral excitation was made near the band gap.

The photon echo results are shown in Fig. 14. Fig. 14 a) corresponds to a polarization parallel to the $\vec{c}$ axis obtained with a sample concentration $x = 0.3$. Three oscillations with 18 fs period are observed as well as a fast initial decay and a much longer decay which lasts during several tens of picoseconds. This slow decay corresponds to a band to band recombination of the carriers after thermalization in the bottom of the conduction and valence bands. It is similar to observations made in bulk GaAs[43]. The initial decay, which lasts about 20 fs (as seen from deconvoluting the slow process) corresponds to the carrier thermalization by intraband energy relaxation. During this process, the phase of the electronic states is being destroyed and coherent oscillations can be observed.
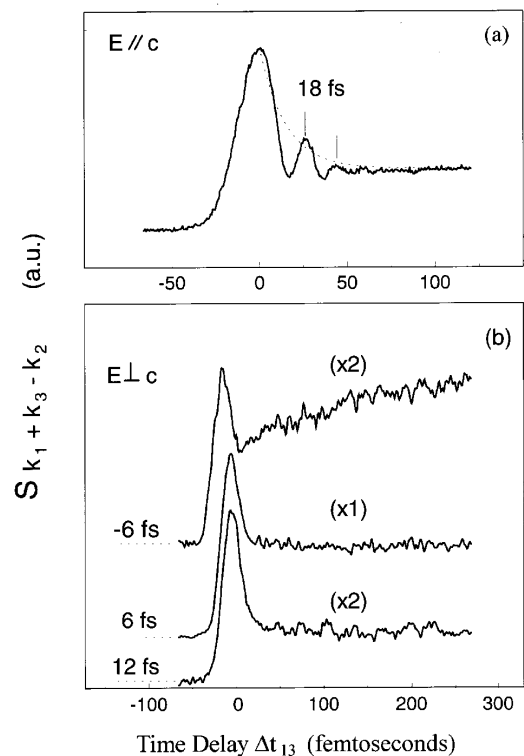

Figure 14. Three-pulse four-wave mixing signals of $CdS_{0.3}Se_{0.7}$ in the two polarizations $\vec{E} \parallel \vec{c}$ and $\vec{E} \perp \vec{c}$ at room temperature and for a carrier density $N = 3 \times 10^{17} cm^{-3}$.

The 18 fs period in Fig. 14 a) corresponds to a quantum beat energy splitting of 230 meV, equal to the energy difference between the A and C valence bands. We therefore attribute these oscillations to interferences between the amplitude transitions corresponding to the interband transitions from the valence bands A and C. This behavior is possible as long as the 10 fs pulse spectrum overlaps the corresponding transitions. This is achieved by choosing the appropriate sample concentration $x = 0.3$ as seen in Fig. 11. In contrast, samples with concentrations which do not verify this overlapping condition display no beating behavior.

Fig. 14 b) shows stimulated echoes obtained for a polarization perpendicular to the $\vec{c}$ axis for three different "phase delays" ΔT_{12}. For a negative ΔT_{12} (− 6 fs), in addition to a strong coherent spike around delay $\Delta T_{13} = 0$, the population increases during several hundred femtoseconds. For $\Delta T_{12} = 6$ and 12 fs, the population stays constant for a very long time and decays later on (not seen on this time scale). This long process corresponds to the radiative band to band recombination. The increasing population for the $\Delta T_{12} = − 6$ fs corresponds to an intraband energy relaxation. Inten-

sity measurements have shown that it is only slightly influenced by the number of electrons and holes and can therefore be related to carrier-phonon scatterings. This mechanism which leads to the thermalization of electrons and holes down to the band edges is much more efficient than in semiconductors like GaAs where longer thermalization times have been reported[44].

In order to further investigate the ultrafast phonon assisted intraband relaxation, we have selectively deposited electron and hole populations with excess energies of about two LO phonons above the band edge. Differential transmission spectra $\frac{\Delta T}{T}(h\omega)$ obtained with the pump-probe technique, are displayed in Fig. 15 for two pump-probe delays $\Delta T_{\rm Pp}$. For $\Delta T_{\rm Pp}$ = 80 fs, a hole burning shows up at the pump energy and almost instantaneously, a population starts to build up down in the band. For the delay $\Delta T_{\rm Pp}$ = 240 fs, the total energy brought by the pump pulse has relaxed at the band edge.
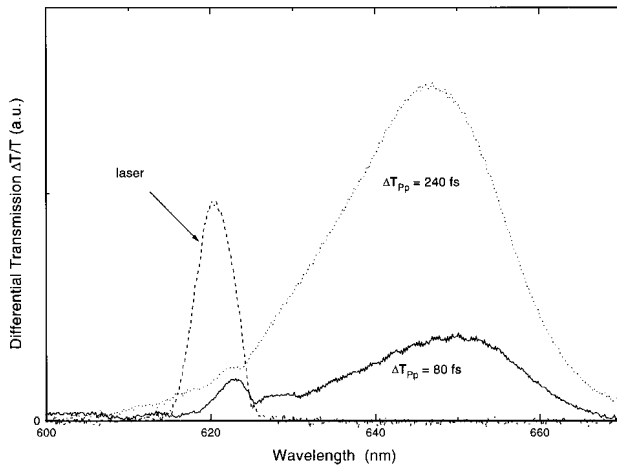

Figure 15. Pump-probe differential transmission spectra $\Delta T/T$ with two different delays $\Delta T_{\rm Pp}$ of 80 and 240 fs between the pump and probe pulses.

These measurements confirm the existence of a very large scattering cross-section for the electron-phonon and hole-phonon interactions. Due to the rather high excess energy of the initial populations, it is the LO phonons which most efficiently participate to this thermalization. However, the acoustic phonons certainly also contribute to the thermalization in a short time scale. This can be seen from the fact that no distinguished LO-phonon replica of the hole-burning is observed indicating an important broadening due to

acoustic phonons. More pump probe studies are being performed on these materials under various experimental conditions in order to quantify the scattering cross-sections and to understand such effects like intervalence band transitions, i.e. A $\longrightarrow$ B transitions.

V. Conclusion

In conclusion, we have reported measurements on the phase dynamics of the localized and extended electronic states in the ternary compounds CdS_xSe_{1-x}. The samples that we studied possess extremely good crystallographic qualities which allowed us to perform a detailed characterization of the localized excitonic states at low temperature. In particular, due to the low elastic scattering, the luminescence obtained under resonant excitation of the localized states can be analyzed directly on the 0-phonon band. In addition, the polarized elastic scattering is seen to be resonant right below the free A exciton. Its spectral shape, as compared to the localized excitonic luminescence and to the absorption in the entire A and B excitonic regions, gives new information on the type of disorder brought by the composition fluctuations. We believe that the fluctuating crystal potential cannot be simply described by a statistic with white noise correlation. The relatively high energetic position of the elastic scattering seems to privilege medium range disorder (on the scale of the exciton Bohr radius).

The dynamical properties of the localized states, studied with pulses of a few hundred femtoseconds duration, clearly reveal two types of mechanisms for the phase and energy relaxation. The first type is a direct consequence of the exciton trapping in the localized wells. It corresponds to both intersite hopping (for the most energetic excitons) and band to band radiative recombination (for the deeper levels). The corresponding dephasing time is very long ($\sim$ 500 ps) as previously reported. The second type is a new mechanism which involves two excitons localized on the same potential wells and which is much faster ($\sim$ 700 fs). Quantum beats with 800 fs period, due to interferences between the transition amplitudes |g> $\longrightarrow$ |ex> and |ex> $\longrightarrow$ |biex>, show up during the coherent decay. This ultrafast decay corresponds to the loss of coherence between the excitonic and biexcitonic states.

Using 10 fs pulses, we also studied the dynamics of the free electrons and holes in the continuum bands at room temperature. This study shows the presence of two mechanisms in the dephasing process. First, the Coulomb scattering leads to density dependent dephasing times. The measurements indicate that this interaction is much less screened than in GaAs. Second, the scattering cross-section of the electron-phonon (and hole-phonon) is very high, leading to an ultrafast intraband thermalization of the carriers. This is observed both with stimulated photon echoes and pump-probe techniques. Such importance of the phonons is probably due to the strong polar character of the CdSSe semiconductors.

The present work brings new information in the understanding of the phase relaxation in non-completely ordered crystals. It leaves opened questions regarding the type of statistics underlying the composition disorder. It also makes further steps towards the difficult task of measuring the phase and energy relaxation in the continua of electrons and holes in semiconductors.

Acknowledgments.

References

1. see, for instance, *Ultrafast Phenomena VIII*, edited by J.-L. Martin, A. Migus, G.A. Mourou and A.H. Zewail (Springer Verlag, Berlin 1993).

2. S. Permogorov, A. Reznitskii, S. Verbin, G.O. Müller, P. Flögel and M. Nikiforova, Phys. Status Solidi (b), **113**, 589 (1982).

3. E. Cohen and M.D. Sturge, Phys. Rev. B, **25**, 3828 (1982).

4. G. Noll, U. Siegner, S.G. Shevel and E.O. Göbel, Phys. Rev. Lett., **64**, 792 (1990).

5. J.-Y. Bigot, A. Daunois, J. Oberlé and J.-C. Merle, Phys. Rev. Lett., **71**, 1820 (1993).

6. A. Daunois, J.-C. Merle and J.-Y. Bigot, J. Appl. Phys., **77**, 429 (1995).

7. P.C. Becker, H.L. Fragnito, C.H. Brito Cruz, R.L. Fork, J.E. Cunningham, J.E. Henry and C.V. Shank, Phys. Rev. Lett., **61**, 1647 (1988).

8. J.-Y. Bigot, M.T. Portella, R.W. Schoenlein, J.E. Cunningham and C.V. Shank, Phys. Rev. Lett., **67**, 636 (1991).

9. O. Goede, L. John and D. Hennig, Phys. Status Solidi (b), **89**, K183 (1978).

10. F.A. Majumder, S. Shevel, V.G. Lyssenko, H.-E. Swoboda and C. Klingshirn, Z. Phys. B, **66**, 409 (1987).

11. C. Gourdon and P. Lavallard, J. Cryst. Growth, **101**, 767 (1990).

12. S. Permogorov and A. Reznitsky, J. Lumin., **52**, 201 (1992).

13. P.W. Anderson, Phys. Rev., **109**, 1492 (1958).

14. N. Hemmat and M. Weinstein, Solid State Sci., **114**, 851.

15. C. Levelut, A. Ramos, J. Petiau and M. Robino, Mater. Sci. Eng. B, **8**, 251 (1991).

16. R. Frerichs, Phys. Rev., **72**, 594 (1946).

17. J.J. Hopfield, J. Phys. Chem. Solids, **15**, 97 (1960).

18. In Refs. 2 and 3, an extra mechanism of population for $E < E_L$ has been considered. It seems to be rather inefficient, except for the region of deep localization which is not the aim of this paper.

19. H. Schwab, V.G. Lyssenko, J.M. Hvam and C. Klingshirn, Phys. Rev. B, **44**, 3413 (1991).

20. C. Gourdon, P. Lavallard, S. Permogorov, A. Reznitsky, Y. Aaviksoo and Y. Lippmaa, J. Lumin., **39**, 111 (1987).

21. Ya. Aaviksoo, Ya. Lippmaa, S. Permogorov, A. Reznitskii, F. Lavallard and C. Gourdon, JETP Lett., **45**, 498 (1987).

22. see for instance, A.M. Weiner, S. De Silvestri and E.P. Ippen, J. Opt. Soc. Am. B, **2**, 654 (1985).

23. L. Schultheis, J. Kuhl, A. Honold and C.W. Tu, Phys. Rev. Lett., **57**, 1797 (1986).

24. S. Weiss, M.-A. Mycek, J.-Y. Bigot, S. Schmitt-Rink and D.S. Chemla, Phys. Rev. Lett., **69**, 2685 (1992).

25. T. Yajima and Y. Taira, J. Phys. Soc. Jpn, **47**, 1620 (1979).

26. S. Shionoya, H. Saito, E. Hanamura and O. Akimoto, Solid State Commun., **12**, 223 (1973).

27. S. Haroche, in *High resolution Laser Spectroscopy*, edited by K. Shimoda (Springer, Berlin 1976), p. 253.

28. P.C. Becker, H.L. Fragnito, J.-Y. Bigot, C.H. Brito Cruz, R.L. Fork and C.V. Shank, Phys. Rev. Lett., **63**, 505 (1989); for a review on beats in molecular systems, see K.A. Nelson and E.P. Ippen, in *Advances in Chemical Physics*, edited by I. Prigogine and S.A. Rice (Wiley, New York 1990), Vol. 75, p. 1.

29. K.P. Cheung and D.H. Auston, Phys. Rev. Lett., **55**, 2152 (1985).

30. V. Langer, H. Stolz and W. von der Osten, Phys. Rev. Lett., **64**, 854 (1990).

31. D.J. Lovering, R.T. Phillips, G.J. Denton and G.W. Smith, Phys. Rev. Lett., **68**, 1880 (1992).

32. E.O. Göbel, K. Leo, T.C. Damen, J. Shah, S. Schmitt-Rink, W. Schäfer, J.F. Müller and K. Köhler, Phys. Rev. Lett., **64**, 1801 (1990).

33. This effect, as well as a detailed analysis of the phase of quantum beats in the case of a multi-photon resonant medium is being submitted for publication.

34. J.-Y. Bigot and B. Hönerlage, Phys. Status Solidi (b), **121**, 649 (1984); ibid. **123**, 202 (1984).

35. W. Eckart and M.I. Sheboul, Phys. Status Solidi (b), **74**, 523 (1976).

36. H. Haug, Phys. Status Solidi (b), **173**, 139 (1992).

37. L. Banyai, D.B. Tran Thoai, C. Remling and H. Haug, Phys. Status Solidi (b), **173**, 149 (1992).

38. K. El Sayed and H. Haug, Phys. Status Solidi (b), **173**, 189 (1992).

39. K. El Sayed, L. Banyai and H. Haug, Phys. Rev. B, **50**, 1541 (1994).

40. R.L. Fork, C.H. Brito Cruz, P.C. Becker and C.V. Shank, Opt. Lett., **12**, 483 (1987).

41. V.L. Gurevich, M.I. Muradov and D.A. Parshin, Europhys. Lett., **12**, 375 (1990).

42. P.C. Becker, D. Lee, A.M. Johnson, A.G. Prosser, R.D. Feldman, R.F. Austin and R.E. Behringer, Phys. Rev. Lett., **68**, 1876 (1992).

43. L. Rota, P. Lugli, T. Elsaesser and J. Shah, Phys. Rev. B, **47**, 4226 (1993).

44. W.H. Knox, C. Hirlimann, D.A.B. Miller, J. Shah, D.S. Chemla and C.V. Shank, Phys. Rev. Lett., **56**, 1191 (1986).